

NRC Publications Archive Archives des publications du CNRC

Through-the-coating writing of tilted fiber Bragg gratings with the phase mask technique

Abdukerim, Nurmemet; Grobnic, Dan; Hnatovsky, Cyril; Mihailov, Stephen J.

This publication could be one of several versions: author's original, accepted manuscript or the publisher's version. / La version de cette publication peut être l'une des suivantes : la version prépublication de l'auteur, la version acceptée du manuscrit ou la version de l'éditeur.

For the publisher's version, please access the DOI link below. / Pour consulter la version de l'éditeur, utilisez le lien DOI ci-dessous.

Publisher's version / Version de l'éditeur:

<https://doi.org/10.1364/OE.27.038259>

Optics Express, 27, 26, pp. 38259-38269, 2019-12-17

NRC Publications Archive Record / Notice des Archives des publications du CNRC :

<https://nrc-publications.canada.ca/eng/view/object/?id=99b24e90-24b1-44a0-862c-2bf3ceebfcd8>

<https://publications-cnrc.canada.ca/fra/voir/objet/?id=99b24e90-24b1-44a0-862c-2bf3ceebfcd8>

Access and use of this website and the material on it are subject to the Terms and Conditions set forth at

<https://nrc-publications.canada.ca/eng/copyright>

READ THESE TERMS AND CONDITIONS CAREFULLY BEFORE USING THIS WEBSITE.

L'accès à ce site Web et l'utilisation de son contenu sont assujettis aux conditions présentées dans le site

<https://publications-cnrc.canada.ca/fra/droits>

LISEZ CES CONDITIONS ATTENTIVEMENT AVANT D'UTILISER CE SITE WEB.

Questions? Contact the NRC Publications Archive team at

PublicationsArchive-ArchivesPublications@nrc-cnrc.gc.ca. If you wish to email the authors directly, please see the first page of the publication for their contact information.

Vous avez des questions? Nous pouvons vous aider. Pour communiquer directement avec un auteur, consultez la première page de la revue dans laquelle son article a été publié afin de trouver ses coordonnées. Si vous n'arrivez pas à les repérer, communiquez avec nous à PublicationsArchive-ArchivesPublications@nrc-cnrc.gc.ca.



Through-the-coating writing of tilted fiber Bragg gratings with the phase mask technique

NURMEMET ABDUKERIM,  DAN GROBNIC, CYRIL HNATOVSKY,*
AND STEPHEN J. MIHAILOV 

National Research Council of Canada, Security and Disruptive Technologies, 100 Sussex Dr., Ottawa, ON, Canada, K1A 0R6

*cyril.hnatovsky@nrc-cnrc.gc.ca

Abstract: Tilted fiber Bragg gratings are inscribed in non-photosensitized single mode fibers through the polyimide coating using a femtosecond infrared laser and a phase mask. The inscription technique used is based on simultaneously translating the fiber along its axis and the focusing cylindrical lens in the orthogonal direction by means of piezoelectric actuators. The grating plane tilt angles up to 10.3° are achieved with a $1.07\ \mu\text{m}$ -pitch phase mask. The cladding modes reach $\sim 5\ \text{dB}$ in strength in transmission despite the presence of the polyimide coating. The effectiveness of the fabricated tilted fiber Bragg gratings for refractive index sensing through the polyimide coating is also demonstrated. Additionally, we show that the classical approach for the inscription of tilted Bragg gratings, which is based on simply tilting the fiber with respect to the interference fringes, cannot be used in tight focusing geometries that are necessary for through-the-coating inscription.

© 2019 Optical Society of America under the terms of the [OSA Open Access Publishing Agreement](#)

1. Introduction

A tilted fiber Bragg grating (TFBG) is a photonic structure inside which tilted periodic planes of refractive index modification are embedded into the fiber core. Tilting the grating planes with respect to the fiber axis results in strong coupling between the core mode and a multitude of back-propagating cladding modes. If the TFBG's spectrum is observed in transmission, the coupling to cladding modes reveals itself through the production of strong resonant dips at discrete wavelengths that are shorter than the core-mode Bragg resonance wavelength [1].

The multiple sensing modalities of TFBGs, which have been widely discussed in the literature [2–4], arise from: i) differential spectral response among the cladding modes and core mode when stress is applied to the fiber and ii) inherent sensitivity of the spectral response of the cladding modes to the environment that surrounds the cladding. Apart from high resolution refractometry, surface plasmon resonance applications and multi-parameter physical sensing (strain, vibration, and temperature) [2–4], TFBGs are used as in-line fiber polarizers and broadband transmission filters [5–8].

Exposure of the fiber core to intense laser radiation is the most common method to fabricate TFBGs (and other types of FBGs). Traditionally, the permanent refractive index change is imprinted into the doped fiber core using an interference pattern formed by two ultraviolet (UV) laser beams. The interference pattern can be produced by either amplitude/wavefront-splitting interferometers or the so-called phase mask technique. When large quantities of identical FBGs are required, the phase mask technique is favored due to its robustness and reproducibility [9].

On the other hand, the use of infrared (IR) femtosecond (fs) lasers for the inscription of different types of FBGs offers a number of advantages over the traditional UV-technology. Namely, FBG inscription with IR fs-lasers does not require i) any photosensitization of the fiber core and ii) removal of the protective polymer (e.g., acrylate or polyimide) coating and, if needed, reapplication of the coating [10–14]. Besides the fact that the latter procedure(s) is technologically involved, especially in the case of polyimide coatings, it introduces structural flaws to the fiber

surface, which weakens the ultimate mechanical strength and long-term reliability of the resultant FBGs.

The inscription of TFBGs using fs-lasers has been demonstrated with different plane-by-plane techniques [15–19] and the phase mask technique [20–22]. However, the inscription of TFBGs inside coated fibers has been limited to a plane-by-plane technique so far [15]. In this respect, showing the capability of using the phase mask technique, which is generally faster, more robust, and more accurate than its plane-by-plane counterpart, for writing TFBGs inside coated fibers is highly desirable for mass production.

In this paper, we demonstrate the inscription of TFBGs using an IR fs-laser and a phase mask in non-photosensitized single-mode silica fibers through the polyimide coating. The required tilt of the Bragg grating planes inside the fiber core is achieved by simultaneously translating the fiber along its axis and the cylindrical lens (that is used to focus the fs-light along the fiber) in the orthogonal direction using piezo-actuated stages. The TFBG tilt angle is then defined by the ratio of translation ranges of the fiber and the cylindrical lens.

We also prove that the classical arrangement used for TFBG inscription with UV-lasers [2], in which it is sufficient to tilt the fiber relative to the fringe pattern, is not suitable for tight focusing geometries that are required for through-the-coating inscription [23–25]. More specifically, we show that even small rotations of the phase mask and/or the cylindrical lens in the plane of diffraction generally split the sharp line-shaped fs-laser focus and, as a consequence, dramatically decrease the peak intensity inside it by reducing the interference fringe contrast and stretching the focal volume along the beam propagation direction. The focal lines can be recombined by counter-rotating the phase mask and the cylindrical lens, but they remain normal to the interference fringes, to which the fiber axis is aligned. Therefore, tilted grating planes cannot be produced by this method inside the fiber core.

2. Background

There are mainly two approaches of fabricating TFBGs with a phase mask and UV light: i) rotating the phase mask and fiber, which also requires the rotation of the focusing cylindrical lens; ii) rotating the phase mask about the beam axis while keeping the phase mask and fiber normal to the incident beam. The inscription is usually performed in photosensitized (i.e., hydrogen/deuterium-loaded) and stripped fibers using a loosely focused UV laser beam [9].

As far as non-photosensitized fibers are concerned, FBG inscription using the phase mask technique is predominantly carried out with IR fs-lasers. However, because of the low photosensitivity of standard fibers at the often-used writing wavelength of 800 nm, the IR fs-laser beam has to be tightly focused in the fiber core through the phase mask [11]. For writing through the fiber coating, the writing beam has to be focused even tighter in order to avoid radiation damage to the fiber coating, which has a much lower damage threshold than silica glass [24]. As analyzed in [25], the confocal parameter of the laser focus inside the fiber should be less than a quarter of the fiber cladding diameter, in order to avoid damage to the protective polymer coating. For such tight focusing geometries, rotation of either the phase mask **M** or the cylindrical lens **CL** results in a focal tilt and split of the interfering diffraction orders, as illustrated in Fig. 1 in the case of rotations in the xz -plane.

When both **CL** and **M** are aligned normal to the incident beam, focal lines of diffracted beams remain parallel to the phase mask, and $+1^{\text{st}}$ and -1^{st} orders have the same diffraction angle $\theta = \arcsin(\lambda/\Lambda_G)$, where λ is the central wavelength of the incident beam, and Λ_G is the phase mask pitch. The diffraction angle θ is counted from the normal to **M**, which in this case coincides with the z -axis. When **M** remains normal to the incident beam and **CL** is rotated by an angle ξ (Fig. 1(a)), the diffraction angles remain the same, but the focal lines of $+1^{\text{st}}$ and -1^{st} orders rotate and separate in space (Δz_{CL} in Fig. 1(a)) along the z -axis (Appendix A and [25]). In the other limiting case, i.e., when **CL** remains normal to the incident beam and **M** is rotated by an

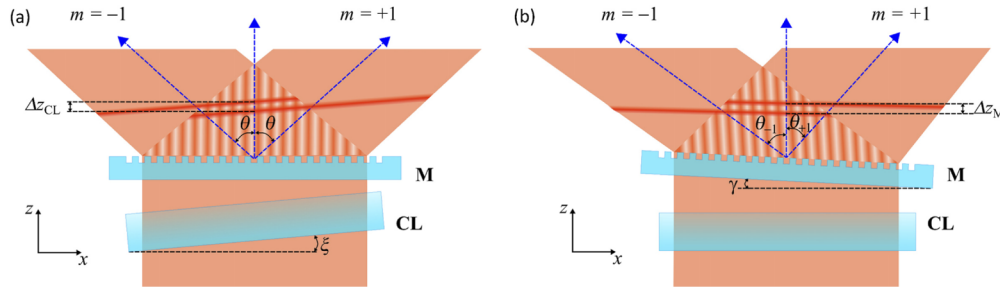


Fig. 1. Illustration of focal tilt and split caused by rotating (a) the cylindrical lens **CL** only (rotation angle ξ in the xz -plane), (b) the phase mask **M** only (rotation angle γ in the xz -plane). **M** produces only 1st diffraction order (i.e., $m = \pm 1$). The respective diffraction angles θ_{+1} and θ_{-1} are counted from the z -axis, which coincides with the beam propagation direction. The focal splits associated with **CL** and **M** rotations are denoted by Δz_{CL} and Δz_M , respectively. A small angle between the split focal lines in (a) and (b) is not shown (see Appendix A).

angle γ (Fig. 1(b)), the diffraction angles (counted from the z -axis) become $\theta_{+1} = \arcsin(\lambda/\Lambda_G - \sin\gamma) + \gamma$ and $\theta_{-1} = \arcsin(\lambda/\Lambda_G + \sin\gamma) - \gamma$, and the focal lines of +1st and -1st orders also rotate and separate in space (Δz_M in Fig. 1(b)) along the z -axis. The focal lines can be recombined by counter-rotating **M** and **CL**. If the angles ξ and γ are small, it can be shown that the focal lines become merged when the condition $\xi/\gamma \approx \tan^2\theta$ is fulfilled (see Appendix A). As an example, the ratio of the angles is ~ 1.26 for a phase mask pitch $\Lambda_G = 1.07 \mu\text{m}$ and a wavelength $\lambda = 800 \text{ nm}$. The recombined focal lines are at an angle $\alpha \approx \gamma/\cos\theta - \gamma$ with respect to the x -axis (see Appendix A).

The interference fringes are formed parallel to the bisector of +1st and -1st-order diffracted beams. In the case of normal incidence, the diffracted beams are symmetric about the beam axis, and the interference fringes are thus parallel to the beam axis. However, when the phase mask is rotated, the bisector is no longer parallel to the incident beam axis. The angle β between the interference fringes and the beam axis (i.e., z -axis) is $\beta \approx \gamma/\cos\theta - \gamma$ under the small-angle approximation (see Appendix A). Therefore, if the focal lines are recombined (i.e., $\xi/\gamma \approx \tan^2\theta$), then $\alpha \equiv \beta$ (for small ξ and γ). Since the fiber axis has to be aligned parallel to the line-shaped focus, grating planes cannot be placed at a practically useful angle inside the fiber as the interference fringes are always perpendicular to the fiber axis.

Rotating the phase mask about the beam axis (i.e., z -axis), while keeping the phase mask and fiber normal to the incident beam, splits the focal lines in the xy -plane along the y -axis. In this situation, the split Δy_M is given by $\Delta y_M = 2z \tan\theta \sin\zeta$, where z is the distance from **M** to the observation xy -plane and ζ is the rotation angle about the z -axis. In the limiting case of $\zeta = 90^\circ$, the diffraction pattern will lie in the yz -plane and the respective focal split will be given by $2z \tan\theta$. For tight focusing, the spot size (at the $1/e^2$ -intensity level) along the y -axis is $\approx 2.5 \mu\text{m}$ [26], and a $\Delta y_M = 2.5 \mu\text{m}$, which at $z = 350 \mu\text{m}$ (see experimental conditions below) corresponds to a mere $\zeta \approx 0.2^\circ$, already separates the focal lines of +1st and -1st orders in the xy -plane and, as a consequence, destroys the interference fringe pattern in the focal volume. This implies, as in in the case of rotations in the xz -plane, that no meaningful tilt angles for grating planes inside the fiber can be achieved for the above mask rotation geometry.

3. Experimental results

Here, we introduce minimum changes to our fs writing setup to produce tilted grating planes in the fiber core. Figure 2(a) illustrates the experimental setup for through-the-coating writing

of TFBGs. Based on our recent studies on complex diffraction and dispersion effects present in the phase mask technique [27], we place the coated fiber at the optimum distance from the phase mask, i.e., where the confocal parameter of the fs-laser focus reaches its minimum. This significantly facilitates through-the-coating FBG inscription, which requires a large differential in intensity between the fiber coating and the fiber core. TFBGs are inscribed by sweeping the laser beam across the fiber core by translating **CL** along the y -axis and simultaneously translating the fiber along the x -axis. Since the fiber itself acts as a cylindrical lens, the refraction of the converging fs-beam at the fiber surface has to be taken into account when calculating the actual translation range of the focus inside the fiber, as shown in Fig. 2(b). This effect was not considered in [21,22], hence the reported tilt angles were grossly underestimated.

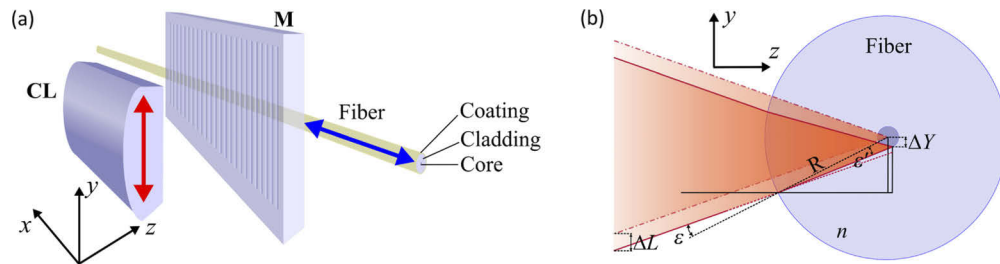


Fig. 2. (a) Experimental setup for writing TFBGs. (b) Refraction of the converging beam at the fiber surface (thin fiber coating is neglected).

Let us assume that the fs-beam is initially focused at the center of the fiber core. In this case the incident rays are normal to the fiber surface. Now let us assume that the fs-beam is moved in free space (i.e., not inside the fiber) by ΔL along the y -axis. The angle of refraction ε' in the fiber is given by Snell's law $\sin \varepsilon' = \frac{\sin \varepsilon}{n}$, where n is the refractive index of the fiber material (silica (SiO_2) in this case) and ε is the angle of incidence, which is no longer 0° .

Under the third-order approximation with respect to ΔL , the transverse movement of the focus inside the fiber is then given by $\Delta Y \approx \Delta L/n$ (see Appendix B). Therefore, the tilt angle of the grating planes ϕ in the fiber core is defined by the ratio of the fiber lateral movement ΔF and the transverse movement of the focus inside the fiber ΔY : $\phi = \arctan(n\Delta F/\Delta L)$. In theory, large angles can be achieved by changing the translation ratio of the fiber and **CL**. However, in practice, a finite spot size of the focus in the fiber core along the y -axis limits the maximum achievable tilt angle ϕ . When the interference fringes with a finite width are moved obliquely in the fiber, the fringe visibility decreases as ϕ increases due to the partial overlap of neighbouring fringes. If the spot size in the fiber is given by $2\omega_1$ (at the $1/e^2$ -intensity level) along the y -axis and the intensity distribution along the x -axis follows the $\cos^2(2\pi x/\Lambda_g)$ -law, the maximum achievable tilt angle will be $\phi_{\max} \sim \arctan(\Lambda_g/4\omega_1)$.

A Ti-sapphire regenerative amplifier operating at a repetition rate of 1 kHz, central wavelength $\lambda = 800$ nm and pulse duration of 80 fs is used in the experiments. The linearly polarized fs-beam is expanded along the x -axis and focused through a zeroth-order-nulled phase mask **M** (Ibsen Photonics) with a pitch $\Lambda_G = 1.07 \mu\text{m}$ using a plano-convex acylindrical lens **CL** with a focal length $f = 15$ mm, with the curved surface designed to correct spherical aberration in one dimension. The linear polarization of the fs-beam is parallel to the mask grooves. Polyimide-coated Corning SMF-28 optical fiber is placed along the line-shaped focus and aligned parallel to **CL**. The fiber is placed $\sim 350 \mu\text{m}$ away from the phase mask, where the confocal parameter of the line-shaped fs-laser focus is smallest and thus the peak intensity in the focus is highest [27]. The position of the laser line focus in the fiber core is aligned by utilizing the techniques of nonlinear photoluminescence microscopy and dark-field microscopy [26]. The piezo-actuated stages for translating **CL** and the fiber are triggered by the same sinusoidal function generator

through a variable power splitter to control the translation ratio along the x - and y -axis. The full swing of the laser focus across the fiber core takes one second. Observations based on the dark-field microscopy technique [28] indicate that the grating fully extends across the fiber core in the z -direction.

The 15 mm length of the TFBGs is defined by the clear aperture of CL. For all the TFBGs, ΔL is kept at 15 μm (which results in $\Delta Y \sim 10 \mu\text{m}$) to cover the entire core. In the case of pure two-beam interference pattern, the period of grating planes along the fiber axis is still given by $\Lambda_G/2$. Hence, TFBGs fabricated with different tilt angles are expected to have their main Bragg resonances positioned at the same wavelength. The TFBG transmission spectra are monitored throughout the writing process using a tunable laser and a power meter with a spectral resolution of 0.01 nm. All the TFBGs are written until saturation upon exposure to the fs-pulses at the pulse energy of 265 μJ for approximately 20 minutes. For our laser-writing conditions, this pulse energy corresponds to a peak intensity of $\approx 1.55 \times 10^{13} \text{ W/cm}^2$ in the fiber core.

Figure 3 shows the transmission spectra of TFBGs written through polyimide coating with different tilt angles up to 10.3°. In each case, the cladding modes reach $\sim 5 \text{ dB}$ in transmission and gradually shift to shorter wavelengths as the tilt angle increases. The cladding modes appear to have an irregular shape due to the presence of the polyimide coating, which has a higher refractive index than silica. The slight variation of the Bragg wavelength is caused by the difference in tension applied while loading the fiber into the fiber-holding jig. We note that when tilt angles are under 4°, the cladding modes are confined within a $\sim 20 \text{ nm}$ wavelength range, allowing the concatenation of multiple TFBGs in a distributed sensing architecture.

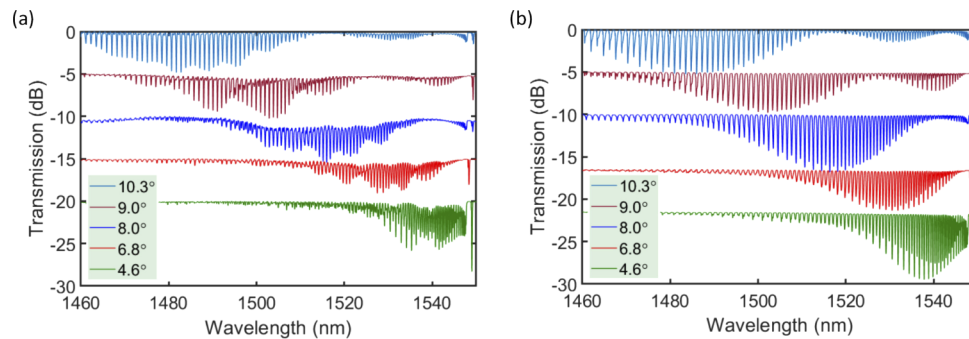


Fig. 3. Transmission spectra of TFBGs written through the coating with different tilt angles of 4.6°, 6.8°, 8.0°, 9.0°, and 10.3°: (a) with the coating, (b) after the coating has been removed. (the spectra are offset along the vertical axis for clarity).

Because the thickness of the polyimide coating is small ($\sim 10 \mu\text{m}$), TFBGs respond well to changes in the surrounding refractive index. As an example, Fig. 4 shows the transmission spectra of a TFBG with a 10.3° tilt angle in response to being immersed in liquids with different refractive indices ranged from 1.317 to 1.440 at room temperature. The accuracy of determining the cut-off wavelength is $\pm 0.7 \text{ nm}$ within the spectral range of 1460–1510 nm, resulting in the surrounding refractive index sensing accuracy of 2.8×10^{-3} . Linear regression based on the TFBG cut-off wavelength λ_c in response to the surrounding refractive index n_{SRI} gives a response function $\lambda_c = 513n_{\text{SRI}} + 804.5$, with $R^2 = 0.9988$. TFBGs with smaller tilt angles (Fig. 3(a)) are expected to preserve this response function for spectral intervals centered at shorter wavelengths.

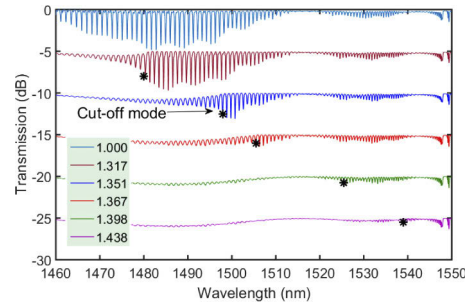


Fig. 4. Transformation of the transmission spectra of a 10.3° TFEBG written through the coating in response to different surrounding refractive indices.

4. Conclusion

In conclusion, through-the-coating inscription of TFEBGs using infrared femtosecond laser and the phase mask technique is demonstrated for the first time. This is achieved using a straightforward technique based on translating the focusing lens and the fiber in orthogonal directions. TFEBGs with the tilt angle of up to 10.3° are fabricated with this method in non-photosensitized SMF-28 fibers coated with a $\sim 10 \mu\text{m}$ -thick layer of polyimide. Accurate analysis of the actual movement of the laser focus inside the fiber is provided using analytical geometry. The effectiveness of through-the-coating sensing of the surrounding refractive index is also demonstrated.

We have also proven that the classical approaches of TFEBG inscription based on tilting the fiber with respect to the interference fringes cannot be used when it comes to tight focusing geometries that are required for through-the-coating inscription. Indeed, we have analytically shown that rotating either the phase mask or cylindrical lens in the plane of diffraction results in the split of the focal lines. Even though the focal lines can be recombined by counter-rotating the phase mask and cylindrical lens, no tilted grating planes can be achieved inside the fiber core due to the intrinsic orthogonality of the recombined focal line and the interference fringes. In this respect, only ‘dynamic’ laser writing, i.e., writing that requires relative translation of the laser focus and fiber, should be employed for through-the-coating inscription of TFEBGs. This is in contrast to the classical approaches that represent ‘static’ laser writing as they do not require any relative translation of the laser focus and fiber.

Appendix A: Analysis of mask and lens rotation in tight focusing geometry

When both the phase mask \mathbf{M} and focusing cylindrical lens \mathbf{CL} are aligned normal to the incident beam, the focal lines of diffracted beams remain parallel to \mathbf{M} , and $+1^{\text{st}}$ and -1^{st} orders have the same diffraction angle $\theta = \arcsin(\lambda/\Lambda_G)$, where λ is the central wavelength of the incident beam, and Λ_G is the phase mask pitch. The diffraction angle θ is counted from the normal to \mathbf{M} , which in this case coincides with the z -axis. Figure 5 illustrates the consequences of rotating either \mathbf{CL} (Scenario 1) or \mathbf{M} (Scenario 2).

In Scenario 1, as shown in Fig. 5(a), \mathbf{CL} is rotated by an angle ξ . Diffraction angles of $+1^{\text{st}}$ and -1^{st} orders remain the same, while the focal lines of $+1^{\text{st}}$ and -1^{st} orders rotate in the same direction as \mathbf{CL} by ψ_{+1} and ψ_{-1} , respectively. The angles ψ_{+1} and ψ_{-1} can be derived based on Fig. 5(a):

$$\psi_{+1} = \arctan\left(\frac{\cos \theta \tan \xi}{1 + \sin \theta \tan \xi}\right), \quad (1a)$$

$$\psi_{-1} = \arctan\left(\frac{\cos \theta \tan \xi}{1 - \sin \theta \tan \xi}\right). \quad (1b)$$

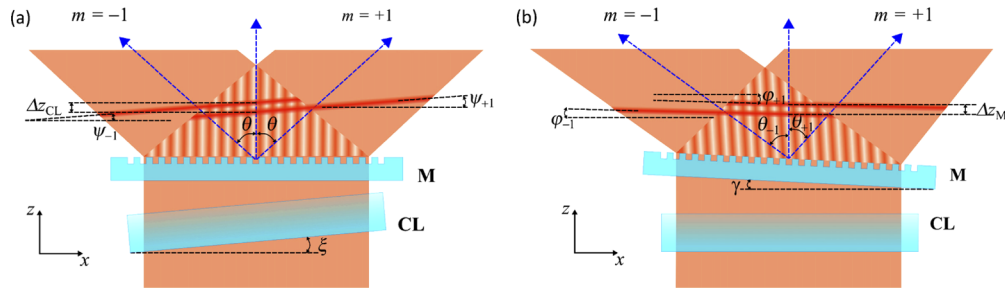


Fig. 5. Illustration of focal split and tilt caused by rotating (a) the cylindrical lens **CL** only, (b) the phase mask **M** only.

Then, the focal split along the z -axis is given by

$$\Delta z_{CL} = z \tan \theta (\tan \psi_{+1} + \tan \psi_{-1}), \quad (2)$$

where z is the distance from **M** to the midpoint between the split focal lines. For small ξ , Eq. (2) reduces to

$$\Delta z_{CL} \approx 2z\xi \sin \theta. \quad (3)$$

In Scenario 2, as shown in Fig. 5(b), **CL** remains normal to the incident beam, while **M** is rotated by an angle γ . In this case, the diffraction angles, which are still counted from the z -axis, become $\theta_{+1} = \arcsin(\lambda/\Lambda_G - \sin\gamma) + \gamma$ and $\theta_{-1} = \arcsin(\lambda/\Lambda_G + \sin\gamma) - \gamma$. As before, the focal lines of +1st and -1st orders rotate in the same direction as **M** by φ_{+1} and φ_{-1} , respectively. The angles φ_{+1} and φ_{-1} can be found using Fig. 5(b):

$$\varphi_{+1} = \arctan \left(\frac{1 - \cos \theta_{+1} \tan \gamma}{1 + \sin \theta_{+1} \tan \gamma} \right), \quad (4a)$$

$$\varphi_{-1} = \arctan \left(\frac{1 - \cos \theta_{-1} \tan \gamma}{1 - \sin \theta_{-1} \tan \gamma} \right). \quad (4b)$$

Then, the focal split along the z -axis is given by

$$\Delta z_M \approx z(\tan \varphi_{-1} - \tan \varphi_{+1})/\cos \theta \quad (5)$$

For small γ , Eq. (5) reduces to

$$\Delta z_M \approx 2z\gamma \sin^2 \theta \tan \theta. \quad (6)$$

Equations (3) and (6) show that for our 1st-order mask the focal splits will be $\Delta z_{CL} \approx 9.1 \mu\text{m}$ and $\Delta z_M \approx 7.7 \mu\text{m}$ per one degree of rotation at $z = 350 \mu\text{m}$, i.e., where the fiber was placed during the inscription. Taking into account that the confocal parameter of our beam in free space is $\approx 11 \mu\text{m}$ at the optimum position $z = 350 \mu\text{m}$ [27], focal splitting caused by introducing ξ or γ at the level of 1° will become comparable with the confocal parameter and, as a result, the interference fringe contrast in the focal volume will be reduced dramatically. In order to have the focal lines overlapped in space at a distance z from **M**, the angles ξ and γ have to satisfy the condition $\Delta z_{CL} = \Delta z_M$ (Eqs. (3) and (6)). For small ξ and γ , the above condition is met when $\xi/\gamma \approx \tan^2 \theta$.

Now we show that the focal lines after **M** can be merged by counter-rotating **M** and **CL**, as shown in Fig. 6, with the angle between **M** and the merged focal lines being denoted by χ .

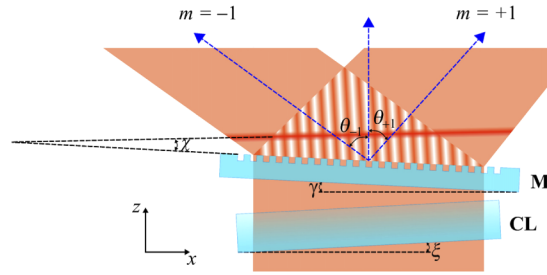


Fig. 6. Merging the focal lines by counter-rotating the phase mask **M** and cylindrical lens **CL**.

The angle χ can be found using the following considerations. The angles shown in Fig. 6 are related to each other as

$$\tan \chi = \frac{\sin(\xi + \gamma) \cos(\theta_{+1} - \gamma)}{\cos \xi + \sin(\xi + \gamma) \sin(\theta_{+1} - \gamma)} = \frac{\sin(\xi + \gamma) \cos(\theta_{-1} + \gamma)}{\cos \xi - \sin(\xi + \gamma) \sin(\theta_{-1} + \gamma)}. \quad (7)$$

By applying the small-angle approximation to Eq. (7), one arrives at the same relationship for ξ and γ , namely $\xi/\gamma \approx \tan^2 \theta$. Finally, for small angles, χ can be written as

$$\chi \approx \gamma / \cos \theta. \quad (8)$$

Therefore, the angle α by which the focal lines are rotated with respect to the x -axis is

$$\alpha = \chi - \gamma = \gamma / \cos \theta - \gamma. \quad (9)$$

When the phase mask is rotated by γ , the angle β between the interference fringes and the z -axis is given by

$$\beta = \frac{1}{2}(\theta_{-1} - \theta_{+1}) \approx \gamma / \cos \theta - \gamma. \quad (10)$$

As one can see, $\alpha \equiv \beta$ for small angles. Therefore, the interference fringes always remain normal to the focal line, to which the fiber is aligned.

Appendix B: Analysis of the laser focus movement inside the fiber

Figure 7 shows the geometry of focusing a fs-beam inside the fiber, with the focusing half-angle being denoted by η . Let us assume that the fs-beam is initially focused at the center of the fiber core, which is represented by the $(0, \Delta L)$ -point. In this case, the incident rays are normal to the fiber surface. The fs-beam is then moved in free space by ΔL along the y -axis. The incident rays a and b are intercepted by the fiber surface at the (z_1, y_1) -point and (z_2, y_2) -point, respectively. Because of the transverse shift ΔL , the rays a and b are now focused at the (z_0, y_0) -point inside the fiber. The angles of incidence and refraction are denoted by ε_1 and ε_2 and ε'_1 and ε'_2 , respectively.

As the fiber surface is represented by a circle of radius R centered at $(0, \Delta L)$, the coordinates of the intercept points (z_1, y_1) and (z_2, y_2) can be found from the circle equation and the slopes of the rays a and b :

$$z_1 = \frac{-\Delta L \tan \eta - \sqrt{R^2 + R^2 \tan^2 \eta - \Delta L^2}}{1 + \tan^2 \eta}, \quad y_1 = -z_1 \tan \eta, \quad (11a)$$

$$z_2 = \frac{\Delta L \tan \eta - \sqrt{R^2 + R^2 \tan^2 \eta - \Delta L^2}}{1 + \tan^2 \eta}, \quad y_2 = z_2 \tan \eta. \quad (11b)$$

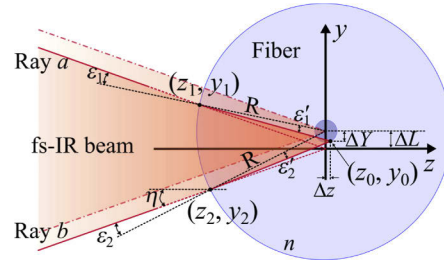


Fig. 7. Illustration of refraction of the converging fs-IR beam at the fiber surface (thin fiber coating is not shown).

The angles of incidence ε_1 and ε_2 are defined with respect to the radial lines that go through (z_1, y_1) and (z_2, y_2) . The slopes of the radial lines are given by

$$\frac{y_1 - \Delta L}{z_1} = \frac{-\tan \eta \sqrt{R^2 + R^2 \tan^2 \eta - \Delta L^2} + \Delta L}{\Delta L \tan \eta + \sqrt{R^2 + R^2 \tan^2 \eta - \Delta L^2}}, \quad (12a)$$

$$\frac{y_2 - \Delta L}{z_2} = \frac{-\tan \eta \sqrt{R^2 + R^2 \tan^2 \eta - \Delta L^2} - \Delta L}{\Delta L \tan \eta - \sqrt{R^2 + R^2 \tan^2 \eta - \Delta L^2}}. \quad (12b)$$

The angles of incidence ε_1 and ε_2 then become

$$\tan \varepsilon_1 = \tan \varepsilon_2 = \frac{\Delta L}{\sqrt{R^2 + R^2 \tan^2 \eta - \Delta L^2}}. \quad (13)$$

The angles of refraction can be found from Snell's law and Eq. (13):

$$\tan \varepsilon'_1 = \tan \varepsilon'_2 = \frac{\Delta L}{\sqrt{n^2 R^2 + n^2 R^2 \tan^2 \eta - \Delta L^2}}, \quad (14)$$

where n is the refractive index of the fiber material. The angles between the refracted rays and the z -axis are $\pi - \eta + \varepsilon_1 - \varepsilon'_1$ and $\eta + \varepsilon_2 - \varepsilon'_2$, respectively. The slopes of the refracted rays are given by quite complicated relationships, which are not shown here. However, if only linear terms of ΔL are retained, the slopes of the refracted rays a and b respectively reduce to

$$\frac{y_1 - y_0}{z_1 - z_0} \approx \left(1 - \frac{1}{n}\right) \frac{\Delta L}{R \cos \eta} - \tan \eta, \quad (15a)$$

$$\frac{y_2 - y_0}{z_2 - z_0} \approx \left(1 - \frac{1}{n}\right) \frac{\Delta L}{R \cos \eta} + \tan \eta. \quad (15b)$$

By knowing the slopes of the refracted rays and the coordinates of points lying on them, one can find the intersection point of the refracted rays, i.e., the focal point inside the fiber. In the linear approximation with respect to ΔL , the coordinates of the focal point are given by

$$z_0 \approx 0, \quad (16a)$$

$$y_0 \approx \frac{(n-1)}{n} \Delta L. \quad (16b)$$

In the quadratic approximation with respect to ΔL , the coordinates of the focal point are

$$z_0 \approx \frac{(n-1)\Delta L^2 \cos \eta}{n^2 R}, \quad (16c)$$

$$y_0 \approx \frac{(n-1)}{n} \Delta L. \quad (16d)$$

Finally, the transverse movement of the focus inside the fiber is

$$\Delta Y = \Delta L - y_0 \approx \frac{\Delta L}{n}, \quad (17)$$

with a high degree of accuracy.

References

1. T. Erdogan and J. E. Sipe, "Tilted fiber phase gratings," *J. Opt. Soc. Am. A* **13**(2), 296–313 (1996).
2. J. Albert, L. Y. Shao, and C. Caucheteur, "Tilted fiber Bragg grating sensors," *Laser Photonics Rev.* **7**(1), 83–108 (2013).
3. X. Dong, H. Zhang, B. Liu, and Y. Miao, "Tilted fiber Bragg gratings: principle and sensing applications," *Photonic Sens.* **1**(1), 6–30 (2011).
4. G. Laffont and P. Ferdinand, "Tilted short-period fibre-Bragg-grating-induced coupling to cladding modes for accurate refractometry," *Meas. Sci. Technol.* **12**(7), 765–770 (2001).
5. K. Zhou, G. Simpson, X. Chen, L. Zhang, and I. Bennion, "High extinction ratio in-fiber polarizers based on 45° tilted fiber Bragg gratings," *Opt. Lett.* **30**(11), 1285–1287 (2005).
6. C. Mou, H. Wang, B. G. Bale, K. Zhou, L. Zhang, and I. Bennion, "All-fiber passively mode-locked femtosecond laser using a 45°-tilted fiber grating polarization element," *Opt. Express* **18**(18), 18906–18911 (2010).
7. R. Kashyap, R. Wyatt, and R. Campbell, "Wideband gain flattened erbium fibre amplifier using a photosensitive fibre blazed grating," *Electron. Lett.* **29**(2), 154–156 (1993).
8. M. Wang, Y. Zhang, Z. Wang, J. Sun, J. Cao, J. Leng, X. Gu, and X. Xu, "Fabrication of chirped and tilted fiber Bragg gratings and suppression of stimulated Raman scattering in fiber amplifiers," *Opt. Express* **25**(2), 1529–1534 (2017).
9. K. O. Hill, B. Malo, F. Bilodeau, D. C. Johnson, and J. Albert, "Bragg gratings fabricated in monomode photosensitive optical fiber by UV exposure through a phase mask," *Appl. Phys. Lett.* **62**(10), 1035–1037 (1993).
10. A. Martinez, M. Dubov, I. Y. Khrushchev, and I. Bennion, "Direct writing of fibre Bragg gratings by femtosecond laser," *Electron. Lett.* **40**(19), 1170–1172 (2004).
11. S. J. Mihailov, C. W. Smelser, P. Lu, R. B. Walker, D. Grobncic, H. Ding, G. Henderson, and J. Unruh, "Fiber Bragg gratings made with a phase mask and 800-nm femtosecond radiation," *Opt. Lett.* **28**(12), 995–997 (2003).
12. A. Martinez, I. Y. Khrushchev, and I. Bennion, "Direct inscription of Bragg gratings in coated fibers by an infrared femtosecond laser," *Opt. Lett.* **31**(11), 1603–1605 (2006).
13. S. J. Mihailov, "Fiber Bragg grating sensors for harsh environments," *Sensors* **12**(2), 1898–1918 (2012).
14. J. Habel, T. Boilard, J. S. Frenière, F. Trépanier, and M. Bernier, "Femtosecond FBG written through the coating for sensing applications," *Sensors* **17**(11), 2519 (2017).
15. A. Ioannou, A. Theodosiou, C. Caucheteur, and K. Kalli, "Direct writing of plane-by-plane tilted fiber Bragg gratings using a femtosecond laser," *Opt. Lett.* **42**(24), 5198–5201 (2017).
16. A. Wolf, M. Kotyushev, A. Dostovalov, and S. Babin, "Femtosecond core-scanning inscription of tilted fiber Bragg gratings," *Proc. SPIE* **10681**, 37 (2018).
17. P. Lu, S. J. Mihailov, H. Ding, D. Grobncic, R. B. Walker, D. Coulas, C. Hnatovsky, and A. Y. Naumov, "Plane-by-plane inscription of grating structures in optical fibers," *J. Lightwave Technol.* **36**(4), 926–931 (2018).
18. J. Tang, C. Fu, Z. Bai, C. Liao, and Y. Wang, "Sensing characteristics of tilted long period fiber gratings inscribed by infrared femtosecond laser," *Sensors* **18**(9), 3003 (2018).
19. G. Bharathan, D. D. Hudson, R. I. Woodward, S. D. Jackson, and A. Fuerbach, "In-fiber polarizer based on a 45-degree tilted fluoride fiber Bragg grating for mid-infrared fiber laser technology," *OSA Continuum* **1**(1), 56–63 (2018).
20. C. Chen, Y. S. Yu, R. Yang, C. Wang, J. C. Guo, Y. Xue, Q. D. Chen, and H. B. Sun, "Reflective optical fiber sensors based on tilted fiber Bragg gratings fabricated with femtosecond laser," *J. Lightwave Technol.* **31**(3), 455–460 (2013).
21. R. Wang, J. Si, T. Chen, L. Yan, H. Cao, X. Pham, and X. Hou, "Fabrication of high-temperature tilted fiber Bragg gratings using a femtosecond laser," *Opt. Express* **25**(20), 23684–23689 (2017).
22. X. Pham, J. Si, T. Chen, F. Qin, and X. Hou, "Wide range refractive index measurement based on off-axis tilted fiber Bragg gratings fabricated using femtosecond laser," *J. Lightwave Technol.* **37**(13), 3027–3034 (2019).
23. S. J. Mihailov, D. Grobncic, and C. W. Smelser, "Efficient grating writing through fibre coating with femtosecond IR radiation and phase mask," *Electron. Lett.* **43**(8), 442–443 (2007).
24. D. Grobncic, C. Hnatovsky, and S. J. Mihailov, "Thermally stable type II FBGs written through polyimide coatings of silica-based optical fiber," *IEEE Photonics Technol. Lett.* **29**(21), 1780–1783 (2017).
25. C. Hnatovsky, D. Grobncic, and S. J. Mihailov, "Through-the-coating femtosecond laser inscription of very short fiber Bragg gratings for acoustic and high temperature sensing applications," *Opt. Express* **25**(21), 25435–25446 (2017).
26. C. Hnatovsky, D. Grobncic, and S. J. Mihailov, "Nonlinear photoluminescence imaging applied to femtosecond laser manufacturing of fiber Bragg gratings," *Opt. Express* **25**(13), 14247–14259 (2017).

27. N. Abdukerim, D. Grobnic, R. Lausten, C. Hnatovsky, and S. J. Mihailov, "Complex diffraction and dispersion effects in femtosecond laser writing of fiber Bragg gratings using the phase mask technique," *Opt. Express* **27**(22), 32536–32555 (2019).
28. C. Hnatovsky, D. Grobnic, D. Coulas, M. Barnes, and S. J. Mihailov, "Self-organized nanostructure formation during femtosecond-laser inscription of fiber Bragg gratings," *Opt. Lett.* **42**(3), 399–402 (2017).